Journal of Power Sources 195 (2010) 1038–1045

Contents lists available at ScienceDirect

Journal of Power Sources

journal homepage: www.elsevier.com/locate/jpowsour

Effects of ionomer content and oxygen permeation of the catalyst layer on proton exchange membrane fuel cell cold start-up

Y. Hiramitsu*, N. Mitsuzawa, K. Okada, M. Hori

Fuel Cell Research Center, Daido University, 10-3 Takiharu-cho, Minami-ku, Nagoya 457-8530, Japan

ARTICLE INFO

Article history:
Received 12 May 2009
Received in revised form 6 August 2009
Accepted 10 August 2009
Available online 15 August 2009

Keywords:
Proton exchange membrane fuel cells
Cold start
Ice
Catalyst layer
Oxygen permeability
Ionomer

ABSTRACT

We have verified the effectiveness of ionomer as a carrier of oxygen to improve cold start-up of proton exchange membrane fuel cells. Galvanostatic cold start was performed on proton exchange membrane fuel cells to evaluate the effect of ionomer content in the catalyst layer on the durability of power generation at −30 °C. Cell voltage and internal resistance were measured, and polarization analysis was conducted to evaluate the cell voltage reduction. Cold start-up durability improved significantly with higher ionomer content in the catalyst layer because of higher oxygen permeation of ice formed in the catalyst layer. These results enable robust design of membrane electrode assemblies for cold start-up.

1. Introduction

Many issues still confront the practical application of proton exchange membrane fuel cells (PEMFCs). In their automotive use, start-up under freezing conditions presents two critical issues. One is that proton conductivity deteriorates considerably at sub-freezing temperatures. The other is that water produced in the cathode by the electrode reaction quickly freezes, which inhibits the diffusion of oxygen to the reaction site on the catalyst through the cathode pores. This freezing of water produced in the cathode pore can cause start-up to fail. Therefore, further improvement for quick, reliable cold start-up is required. PEMFC systems for automotive use should at least match the cold start-up performance of current gasoline-powered vehicles [1].

In order to improve the cold start-up of PEMFC systems, many studies have been performed. Some of these studies reported the possibility of a cold start-up based on test results from single cells or a short stack without countermeasure at temperatures below freezing [2–5]. In these reports, the fundamental cell performance at sub-freezing temperatures for non-isothermal start-up were investigated, and the importance of heat balance between the heat capacity of the cells and the heat of reaction were emphasized. Of course, there is a very large difference in the heat balance between a stack and a single cell [6–8].

Under both non-isothermal and isothermal conditions, water transport during cold start-up was calculated by Jiang et al. [9]. This study indicated that water movement due to a temperature increase was the critical influence on start-up performance. In addition, the continuous generation time was prolonged by optimizing the operational conditions during cold start-up. To understand the phenomena of freezing in the cell, visualization experiments were performed by Ge and Wang [10] and Ishikawa et al. [11–14]. These reports elucidated the existence of product water in a supercooled state at an operational temperature of −10 °C. Ishikawa et al. visualized the cross-section of the cell, and found that cell performance degraded when the supercooled state of the water was broken, which resulted in freeze propagation along the interface between the gas diffusion layer (GDL) and the catalyst layer (CL) [13,14]. Furthermore, analysis was performed to observe ice formation and distribution in the CL during cold start-up at −25 °C with a cryostat-scanning electron microscope by Li et al. [15]. They succeeded in capturing the distribution of ice/frost in the cross-section of a membrane electrode assembly (MEA). There were more ice bridges in the pores of the CL close to the carbon sub-layer than in the CL close to the membrane. They reported that this resulted from the movement of the water due to partial ice thawing, which was attributed to a locally higher temperature due to reaction and ohmic heating.

Cyclic voltammetry was applied to the study of ice formation in the CL by Ge and Wang [16] in the temperature range from −10 °C to −30 °C. It was found that the electrochemical surface

* Corresponding author. Tel.: +81 52 612 6144; fax: +81 52 612 6144.
E-mail addresses: hiramitu@daido-it.ac.jp (Y. Hiramitsu), sc_xt1581f@yahoo.co.jp (N. Mitsuzawa), sasugadayona_orera_neet@ezweb.ne.jp (K. Okada), hori@daido-it.ac.jp (M. Hori).

0378-7753/$ – see front matter © 2009 Elsevier B.V. All rights reserved.
doi:10.1016/j.jpowsour.2009.08.016

area decreased with the formation of ice. They reported that liquid water was trapped between Pt particles and ionomers as a result of ice melting because of local heat production by power generation. In order to evaluate cell performance under severe conditions, simulation analysis and determination of the cell voltage, current density, and cell resistance were performed on cells in the temperature range from −10 °C to −30 °C. These studies mainly focused on the cell voltage, cell resistance, mass transport, and structural parameters of the CL with ice [15–26]. Chacko et al. [26] reported that the cell resistance initially decreased due to CL ice removal, then increased due to membrane dehydration at −10 °C. They also reported that lower start-up current densities can produce more water than the theoretical capacity of the cathode CL, because of the removal of supercooled water from the CL. New insights were reported regarding the relationship between local water accumulation/removal and cell performance. Oszcipok et al. [22] reported that membrane/contact resistance decreased and charge transfer resistance increased significantly based on simultaneous AC impedance spectroscopy during cold start-up at −10 °C. Hou et al. reported that the ohmic resistance did not change, regardless of freezing, and that the mass transport resistance significantly increased with increasing residual ice, even at a small current density. They also found that irreversible performance degradation resulted from water freezing in the pores and disrupting the pore structure at −10 °C [23].

The influence of the initial water content in a membrane on cold start-up performance was investigated at −10 °C to −30 °C by Tajiri et al. [24,25]. They reported that product water moved from the CL to dry membrane in the early stage of cold start-up. Furthermore, Tajiri et al. reported a close relationship between cold start-up reliability, purge time, membrane thickness, and current density. They concluded that a cell stack could be easily started-up below the freezing point of water by incorporating a perfect dry purging process into the stop sequence of fuel cell operation and by increasing the thickness of the membrane. Their results suggested an effect of current density on water accumulation in the CL. In fact, when their cell started-up at a higher current density, the pores in the CL were incompletely flooded with product water [24].

For practical application in an automobile at sub-freezing temperatures, a gas purge procedure is performed during the shutdown process to avoid ice formation, which would block gas flow and diffusion. Tajiri et al. [27] discussed water removal from MEA during purging by analyzing the time variation of the membrane resistance. Furthermore, Lee et al. [28] developed a technique to measure the quantity of water remaining after purge in a stack.

In summary, many studies have addressed the behavior of water, ice, and/or frost produced during cold start-up in fundamental single-cell studies. However, all studies on cold start-up have arrived at the same conclusion on how to diffuse oxygen to the reaction site of Pt catalyst through the electrode pores, especially through the cathode CL pores which can be blocked by ice formation during cold start-up. On the other hand, independent of cold start-up, it is generally believed that oxygen dissolves into an ionomer after diffusion through pores in the CL, and that it diffuses onto the surfaces of Pt particles through the ionomer [22–25,29]. To investigate this oxygen transport process, oxygen solubility and diffusion coefficient in Perfluorosulfonic Acid (PFSA) were measured using an electrochemical method [30,31]. Büchi et al. indicated that the oxygen solubility increases with increasing hydrophobicity of the polymer electrolyte membrane, but that the oxygen diffusivity relates to the water content and chemical structure of the proton exchange membrane (PEM) [30]. Furthermore, Mitsushima et al. indicated that the oxygen diffusion coefficient is closely dependent on the equivalent weight (EW), and that oxygen solubility and permeability can be improved by decreasing the EW [31]. Mohamed et al. suggested that oxygen permeation in Nafion is dominated by its free volume in the relative humidity (RH) region below 60%, and that it is dominated by water uptake, which is related to molecular motion in the RH region above 60% [32].

Although there have been several studies on oxygen transport through ionomer, there has been no report discussing this transport in connection with cold start-up. Below the freezing point, oxygen transportation in the ionomer may not sharply decrease but rather slightly increase due to hydration of the ionomer. Therefore, during cold start-up, oxygen transport through the ionomer may become dominant in the CL when its pores are partially filled with ice. Taking the above-mentioned situations into consideration, we have undertaken studies on the cold start-up of PEMFCs with a focus on oxygen transport through the ionomer. In this work, the influence of oxygen transport in the ionomer on cold start-up was examined by conducting in situ and ex situ cold start-up tests on PEMFC single cells and sub-cells, respectively.

To perform in situ cold tests, power was generated from three single cells with varying ionomer content in a freezer at a temperature of −30 °C. The possibility of cold start-up was evaluated, based on the time during which the cells continued to generate electric power at a constant current density. Ex situ cold tests were performed to quantitatively evaluate the oxygen transport rate through the ionomer at sub-zero temperatures. Elemental generation tests were conducted with a potentiostat–galvanostat on the sub-cell with a cathode consisting of ionomer-coated Pt mesh and the usual anode consisting of carbon black-supported Pt catalyst and ionomer.

2. Experimental

2.1. In situ test

2.1.1. Preparation of single cells with different amounts of ionomer

A 50-μm-thick Nafion membrane (NRE212CS, Dupont) with EW = 1100 g mol.$^{-1}$ was used as a PEM. Pt catalyst supported by carbon black (TEC10E50E, Pt/C weight ratio of 46/54, Tanaka Kikinzoku Kogyo K. K., Japan) was used as both the anode and cathode catalyst. Nafion solution (DE-520CS, Dupont) was used as the ionomer. Three kinds of catalyst inks with ionomer/carbon black weight ratios (I/C) of 0.5, 1.0, and 1.5 were prepared by mixing the catalyst with the Nafion solution.

The catalyst inks obtained were applied to a Polytetrafluoroethlene (PTFE) sheet. The CL with I/C of 0.5, 1.0 and 1.5 were fabricated at Pt catalyst loadings of 0.30, 0.26 and 0.25 mg cm^{-2}, respectively, for both anode and cathode. PEM sandwiched with two sheets of ink-applied PTFEs was hot-pressed at 150 °C at a pressure of 4.9 MPa for a few minutes. Fig. 1 shows a detailed view of a single cell prepared for the in situ cold test. The obtained catalyst-coated membrane (CCM) with a PEM and CL was sandwiched between two sheets of GDLs (TGP-H-090, Toray Industries Inc., Japan) with areas of 30 mm × 3 mm and 30 mm × 30 mm for the cathode and anode sides, respectively. Hydrophobic pretreatment was performed on the GDLs by dipping in 12 wt% PTFE dispersion (31-JR, DuPont-Mitsui Fluorochemicals Co. Ltd, Japan) and by heating at 350 °C for several minutes. MEA thus obtained with a CCM and two sheets of GDLs were tightly fastened together with two graphite flow fields (Nippon Carbon Co. Ltd., Japan) and two stainless steel end plates.

2.1.2. Cold power generation test

The single cells were set in a freezer (SU-241, Espec Corp., Japan) after drying in a forced convection oven (DRM420DA, Toyo Seisakusho Kaisha, Ltd., Japan) for over 30 min. Fig. 2 shows a schematic diagram of the power generation equipment for the in situ cold test. As shown in the figure, the cell temperature was controlled by the surrounding temperature in the freezer. Flow rates

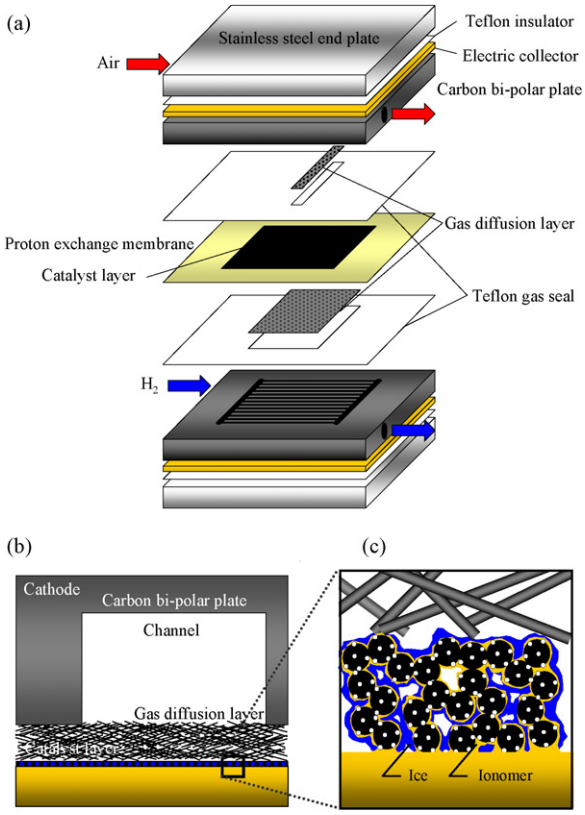

Fig. 1. Detailed view of a single cell prepared for the in situ cold test. (a) shows the cell assembly, (b) shows the cathode cross-section, and (c) shows an expanded image of the gas diffusion electrode.

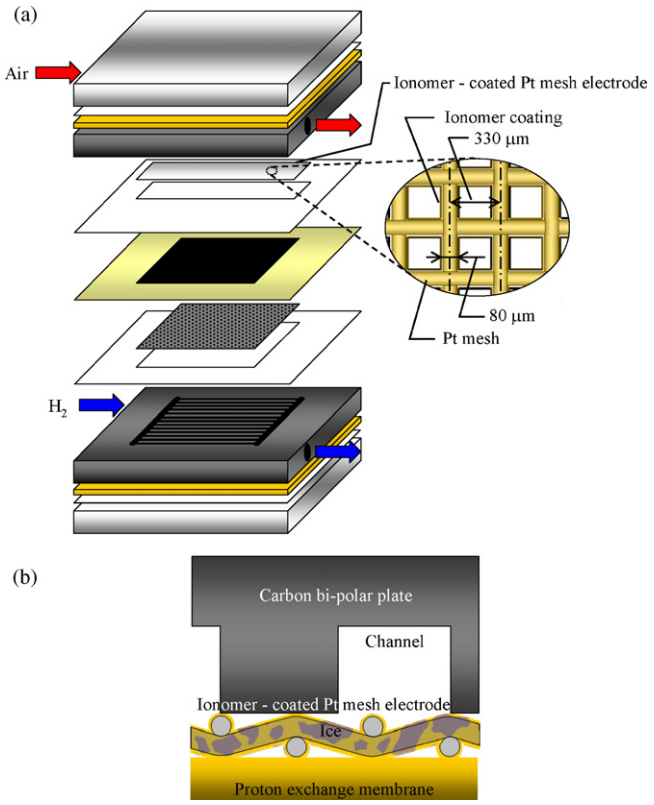

Fig. 3. Detailed view of a single cell prepared for the ex situ cold test. (a) shows the cell assembly and an expanded image of the ionomer-coated Pt mesh electrode and (b) shows the cathode cross-section and elemental gas diffusion electrode using an ionomer-coated Pt mesh electrode.

of fuel and oxidant were controlled by mass flow controller (5850 i, Emerson Japan, Ltd., Japan). The RH of anode and cathode gases was controlled by a saturation method. The humidifier consisted of ice saturators whose temperature was controlled by a water-cooled Peltier unit (PU-50W, Takagi MFG. Co. Ltd., Japan) cooling system and a cooled mirror hygrometer (Finedew, Yamatake Corp., Japan). Cell currents were set at their designated value with a potentiostat–galvanostat (HZ-5000, Hokuto Denko Corp., Japan). High-frequency resistance was simultaneously measured with a 10 kHz ohmmeter (FC-100R, CHINO Corp., Tokyo, Japan) as the cells' internal resistance (IR) during cold power generation.

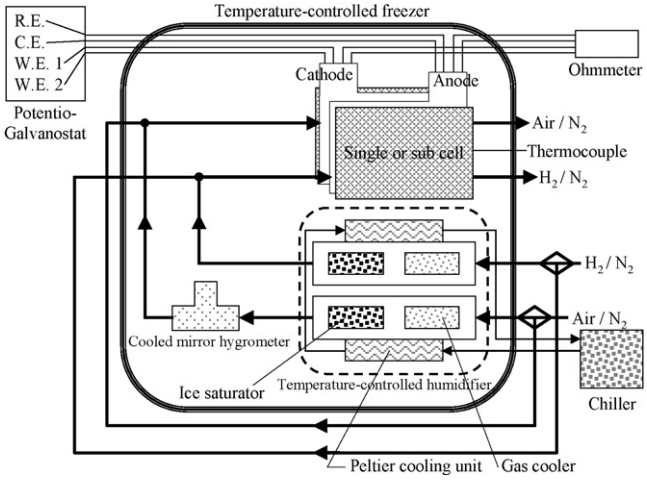

Fig. 2. Schematic diagram of the fuel cell test stand for cold test operation. R.E.: reference electrode; C.E.: counter electrode; W.E. 1: working electrode to load; W.E. 2: working electrode to measure the cell voltage.

The cells were first cooled to the in situ cold test temperature of −30 °C under dry N_2 flow of 0.1 L min^{-1} at both the anode and cathode. Secondly, the gas was switched from N_2 to H_2 flow at 0.095 L min^{-1} at the anode and air flow at 0.117 L min^{-1} at the cathode. The H_2 and air were humidified to 54% RH. The cells were kept under these conditions for several minutes until the open circuit voltage (OCV) stopped increasing. Next, the cell was discharged at a sweep rate of 0.5 mA cm^{-2} s^{-1} to 40 mA cm^{-2}. This cold start procedure was repeated two to five times.

2.2. Ex situ test

2.2.1. Preparation of sub-cell with Pt mesh cathode catalyst

For ex situ elemental testing, two sub-cells were prepared. Fig. 3 shows a detailed view of the sub-cell prepared for quantitative evaluation of oxygen permeation through the ionomer. The sub-cells had an anode consisting of carbon-supported Pt catalyst and ionomer with an I/C of 1.5 and a cathode consisting of ionomer-coated Pt mesh (Furuya Metal Co. Ltd., Japan) for which the surface area could be defined differently from the actual carbon-supported Pt catalyst. Instead of the CL and GDL generally used for the cathode, Pt mesh was employed to enable better estimation of the oxygen transport rate through the ionomer by evaluating the change in current. The cathode active area in the sub-cell was 10 mm × 40 mm. The Pt wire interval was 330 μm, and the Pt wire diameter was 80 μm. Ionomer was coated onto the Pt wire mesh surface by a repeated sequence of dipping into 1 wt% ionomer solution, drying, and weighing with a precision electronic balance (AUW120D, Shimadzu Corp., Japan). The thickness of ionomer coating on the Pt wires was calculated by the following Eq. (1):

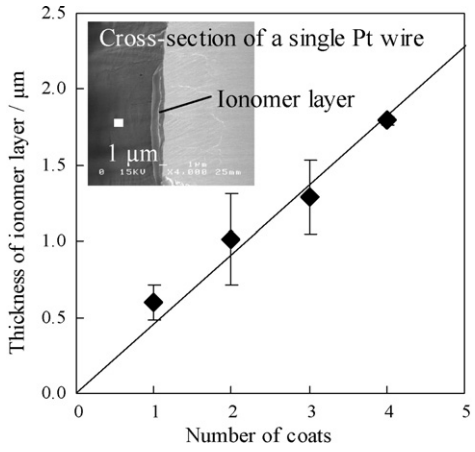

Fig. 4. The relationship between the number of applications of the coating process and the ionomer thickness. The concentration of the ionomer solution was 1 wt%. The thickness of the ionomer coating was estimated geometrically by Eq. (1). Inset shows the cross-section of a single wire from the Pt mesh, obtained using a scanning electron microscope.

$$T_{ionomer} = \sqrt{\frac{ML_1}{2\pi\rho L_2 L_3} + \left(\frac{d}{2}\right)^2} - \frac{d}{2} \quad (1)$$

where M is the coated ionomer weight, L_1 the lattice interval of Pt mesh, L_2 the length of one side of Pt mesh, L_3 the length of other side of Pt mesh, ρ the density of ionomer, and d is the diameter of Pt wire. Fig. 4 shows the relationship between the ionomer thickness calculated by Eq. (1) and the number of repetitions of the ionomer coating process. As shown in the figure, there was a linear relationship between the amount of ionomer and the number of coats applied.

2.2.2. Ex situ cold test of the sub-cell with ice accumulation at −30 °C

Firstly, the Pt mesh electrode was preconditioned with potential scan in the range from 0.08 V to 1.2 V with the same potentiostat–galvanostat as in Section 2.1.2 at a sub-cell temperature at 80 °C under saturated water vapor condition with 0.1 L min^{-1} of H_2 at the anode and 0.1 L min^{-1} of N_2 at the cathode to refresh the surface of the electrode.

After preconditioning, the sub-cell was dried in a forced convection oven. After drying, the sub-cell was cooled to −30 °C with dry N_2 at 0.1 L min^{-1} at both the anode and cathode on the power generation test stand, which was the same equipment shown in Fig. 2. The gas was switched from N_2 to H_2 at 0.031 L min^{-1} and air at 0.075 L min^{-1} at anode and cathode, respectively, and both process gasses were previously humidified to 64% RH. After the sub-cell was kept in this state for several hours until the OCV stopped increasing, the cell voltage applied to the sub-cell was decreased from OCV to 0.1 V at a sweep rate of −5 mV s^{-1} with linear sweep voltammetry (LSV) to evaluate the polarization. Then, galvanostatic generation was performed to accumulate ice around the electrode. A current density was applied from zero to 80 μA cm^{-2} at a rate of 20 μA cm^{-2} s^{-1}, in a staircase pattern, and was then kept constant at 80 μA cm^{-2} for 1250 or 5000 s. After constant current power generation, LSV was performed to evaluate polarization with ice accumulation. The LSV was conducted at sweep rate of −5 mV s^{-1}. These two sequences of operation were repeated in the measurements. In parallel, high-frequency resistance was also measured with a 10 kHz ohmmeter (FC-100R, Chino Corp., Tokyo, Japan) as cell IR during the measurements.

3. Results

3.1. In situ test

Fig. 5 shows the time change of the cell voltages and IRs obtained from the in situ power generation tests conducted on three single cells with I/C of 0.5, 1.0, and 1.5. The results shown for the cell with I/C = 0.5 is the 4th generation step and the others are the 1st generation step.

As shown in Fig. 5, the time change of the cell voltages obtained from the in situ tests of cells with I/C of 1.0 and 1.5 roughly consisted of three distinct regions. In the 1st region, from the beginning to 80 s, increasing the current up to a density of 40 mA cm^{-2} at the slow sweep rate of 0.5 mA cm^{-2} s^{-1}, caused the cell voltage to rapidly decrease. The decrease in cell voltage was less marked for the cell with higher I/C than for the cell with lower I/C.

In the 2nd region, while the current was maintained at 40 mA cm^{-2}, the cell voltage gradually increased along with a gradual decrease in cell IRs. This region tended to become longer for the cell with higher I/C than for the cell with lower I/C. In this region, the cell voltage reached a peak, and then slightly decreased. After cell IR bottomed out, the 3rd region began. In the 3rd region, the cell voltage declined to zero at the constant current of 40 mA cm^{-2} with an increase in resistance. This region also tended to become longer for the cell with higher I/C than for the cell with low I/C.

An extremely long generation duration was obtained for the cell with I/C of 1.5, indicating that even if ice grows and distributes among the pores of the CL, oxygen transport still occurs, and the ionomer serves as the path of oxygen transport from the GDL to the catalyst reaction site. Thus, the oxygen permeability through the ionomer is larger than that of ice, and is sufficient to generate 40 mA cm^{-2}.

Fig. 6 shows the result of the in situ cold test of the cell with I/C = 0.5 as the relationship of cell voltage and cell IR to integrated product water. As shown in Fig. 5 cold power generation cycles were performed using the cell with an I/C = 0.5. With each successive generation, the OCV increased and the cell resistance decreased. The 4th cold power generation was the first time the cell was able to generate at the constant current of 40 mA cm^{-2} over 80 s. Based on the results in the figure, it was presumed that the water produced by the generation reaction was absorbed into both the PEM and ionomer, that the cell IR gradually decreased, that the catalyst activation increased with the increase in the effective triple phase boundary, and that the OCV increased with each successive cold power generation.

In the next section, the oxygen permeability through the ionomer under ice accumulation was verified using the ex situ test.

3.2. Ex situ test

Fig. 7(a) and (b) shows the results obtained from the ex situ tests, on sub-cells with a cathode consisting of a Pt mesh on which ionomer 1000 or 1500 nm thick was coated. The figure depicts the relationship between current density and IR-free cell voltage. The two curves in Fig. 9(a) and (b) show typical results of polarization curve analysis for 10 μm cm^{-2} and 900 μm cm^{-2} of integrated water, as calculated by Eq. (2), respectively. IR-free cell voltage $E_{IR\text{-free}}$ corrected by Eq. (3) is shown on the horizontal axis.

$$m_{H_2O} = \frac{M_{H_2O}}{2F} \int i\,dt \quad (2)$$

where m_{H_2O} is the quantity of matter of product water, M_{H_2O} the molecular weight of water, F the Faraday's constant, i the current density, and t is the time.

$$E_{IR\text{-free}} = E + Ri \quad (3)$$

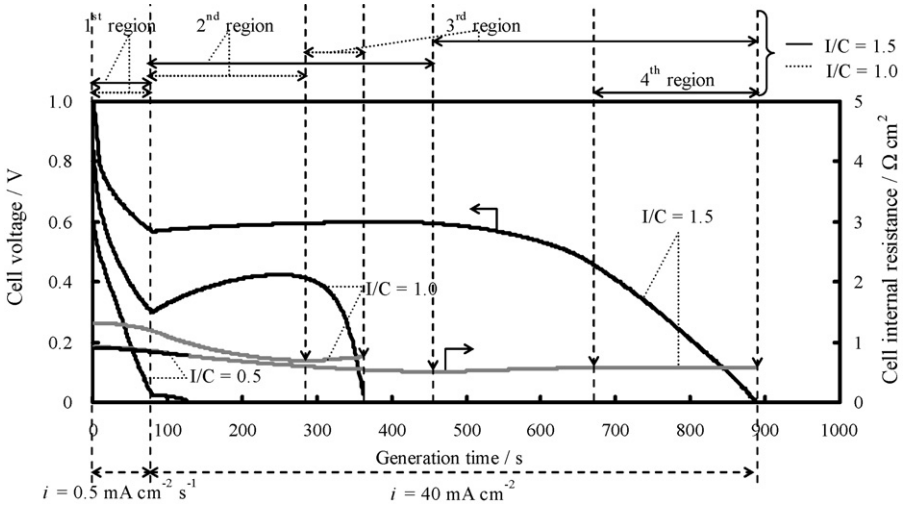

Fig. 5. Time change of cell voltage and cell resistance for various I/C ratios. The cell was discharged at a sweep rate 0.5 mA cm^{-2} s^{-1} to 40 mA cm^{-2} and then 40 mA cm^{-2} constantly. The cell temperature was −30 °C, and the dew point of the humidified gas was −33 °C. The current density was described in absolute value.

where $E_{\text{IR-free}}$ is the IR-free cell voltage, E the cell voltage, R the cell IR, and i is the current density.

Oxygen diffusion inhibition by ice accumulation over the Pt mesh electrode was evaluated using the diffusion overpotential, which was obtained by polarization analysis. The polarization analysis was performed to fit the experimental I–V curves by Eq. (4) using the least-squares method. The diffusion overpotential $\eta_{\text{diffusion}}$ was calculated by Eq. (5).

$$E = E_{\text{OCV}} - b_1 \ln\left(\frac{i}{i_0}\right) - b_2 \ln\left(\frac{i_{\text{lim}}}{i_{\text{lim}} - i}\right) - Ri \tag{4}$$

$$\eta_{\text{diffsion}} = b_2 \ln\left(\frac{i_{\text{lim}}}{i_{\text{lim}} - i}\right) \tag{5}$$

where E is the cell voltage, E_{OCV} the open circuit voltage, b_1 the Tafel slope at low current density, i the current density, i_0 the exchange current density, b_2 the Tafel slope at high current density, i_{lim} the limiting current, R the cell resistance, and $\eta_{\text{diffusion}}$ is the diffusion overpotential. The theoretical E_{OCV} of 1.23 V was used. Instantaneously measured high-frequency resistance was used as the cell IR R. In the polarization curve analysis, the anode polarization and change in hydrogen crossover during measurement were neglected. The polarization analysis results agreed well with the experimental data.

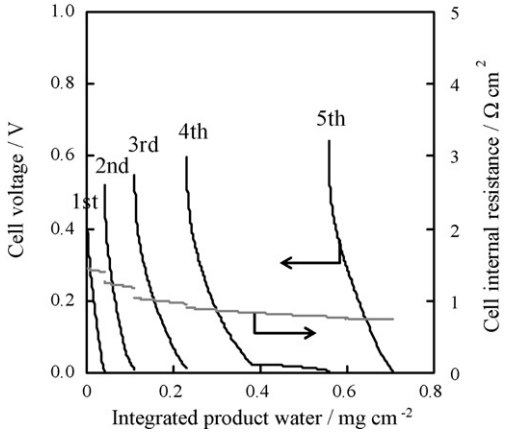

Fig. 6. Relationship of cell voltage and cell IR to integrated product water for I/C = 0.5 with multiple in situ cold tests.

Fig. 8 shows the relationship of the diffusion overpotential $\eta_{\text{diffusion}}$ at 50 μA cm^{-2} to the integrated product water, which was obtained by polarization analysis, with results shown in Fig. 7. As shown in the figure, $\eta_{\text{diffusion}}$ tended to increase with increasing integrated product water. This result indicates that the product

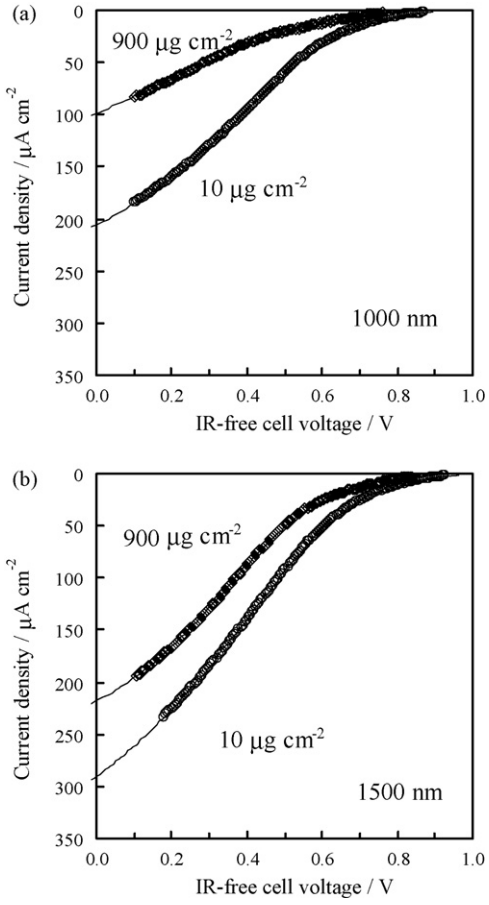

Fig. 7. Typical LSV curves, which depended on the thickness of ionomer coated on the surface of the Pt mesh of 10 μm cm^{-2} and 900 μm cm^{-2} representing less and more integrated product water, respectively. The cell temperature was −30 °C, and the dew point of the humidified gas was −31.5 °C, respectively. The current density was described in absolute value.

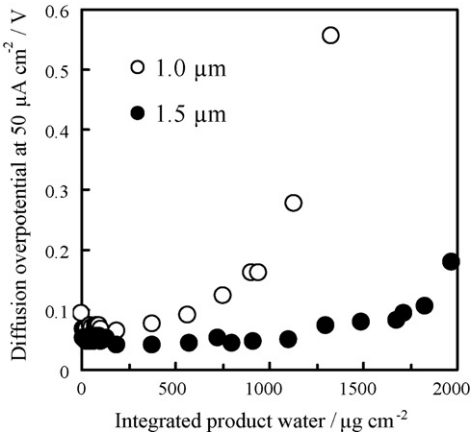

Fig. 8. Relationship of diffusion overpotential $\eta_{diffusion}$ to integrated product water obtained by the generation test at −30 °C. Hollow and solid symbols indicate the respective ionomer thickness of 1.0 μm and 1.5 μm on the surface of the platinum mesh electrodes.

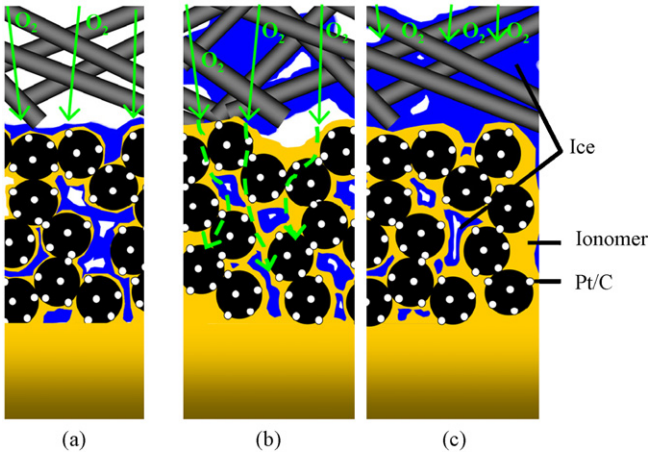

Fig. 10. Schematic image of oxygen transport under ice accumulation on the cathode. (a) shows small I/C, (b) shows large I/C in the 4th region of Fig. 5 and (c) shows large I/C of 1.5 at about 900 s in Fig. 5.

water froze around the Pt mesh electrode, blocking oxygen diffusion to the Pt mesh surface. Furthermore, this result confirms that $\eta_{diffusion}$ decreased in proportion to the increase in thickness of the ionomer coated on the Pt mesh electrode.

4. Discussion

4.1. Influence of ionomer water absorption on cell voltage

In the 2nd region shown in Fig. 7, the IR of the cells with I/C = 1.0 and 1.5 decreased, which was consistent with the results of Tajiri et al. [24] and Chacko et al. [26]. They reported that the decrease in IR in this region was caused by water movement from the CL to the PEM. Tajiri et al. found that the generation time was prolonged by reducing the initial water content in the PEM [24].

On the other hand, the results shown in Section 3.1 demonstrate that the increase in cell voltage and the decrease in IR in the 2nd region were dependent not only on the initial water content of the PEM but also on the I/C of the CL. Furthermore, it seems reasonable that there is a correlation between the increase in cell voltage and the decrease in IR in the 2nd region. Fig. 9 shows the relationship between the temporal differentials of cell voltage E and

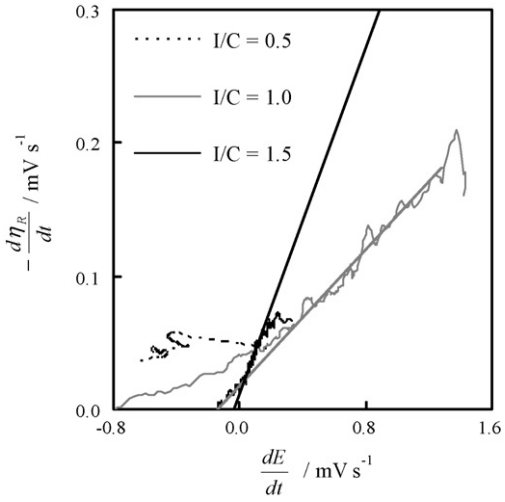

Fig. 9. Relationship between numeric temporal differential of cell voltage E and numeric temporal differential of $-\eta_{resistance}$ in the second region of Fig. 5.

resistance overpotential $-\eta_{resistance}$, in the 2nd region. A linear relationship was found between both differentials, which suggests that the recovery of cell voltage in the 2nd region was directly related to the decrease in $\eta_{resistance}$, which is thought to be affected by water movement from the CL to the PEM. When the ratio, the slope in Fig. 9, of the temporal differential of $\eta_{resistance}$ to that of E was equal to 1.0, the resistance overpotential dominated the cell voltage, and was much more significant than the other overpotentials. However, Fig. 9 also shows that the ratios were, at most, 0.13 and 0.32 for the cells with I/C = 1.0 and 1.5, respectively. This indicates that the effect of the other overpotentials on the cell voltage cannot be neglected.

Among these other overpotentials, the activation overpotential $\eta_{activation}$ is particularly influential. It is thought that water in the ionomer plays a role in the transfer of protons to the reaction site of the Pt catalyst. The amount of water in the ionomer is also thought to affect the utilization of the Pt catalyst, the activation overpotential, and the cell voltage. Of course, the high I/C allows the ionomer to contain a large amount of water. This is supported by the observation that the ratio of $-d\eta_{resistance}/dt$ and dE/dt increases with increasing I/C in the CL. On the other hand, in the cell with I/C = 0.5, as $\eta_{resistance}$ decreased, the cell voltage decreased with increasing OCV shown in Fig. 8. This suggests the existence of oxygen diffusion overpotential.

Fig. 10(a)–(c) shows conceptual diagrams of the CLs of I/C = 0.5, 1.0, and 1.5, respectively. As shown in (a) for the cell with an I/C = 0.5, it is thought that in the CL, ice covered the ionomer surface in the early stages, preventing oxygen gas diffusion from the CL pores to the reaction sites of the Pt catalyst, and that the diffusion overpotential, $\eta_{diffusion}$, became dominant.

4.2. Influence of oxygen transfer function of ionomer on power generation time

The power generation time can be prolonged by heightening the I/C of the CL, as shown in Fig. 5. Tajiri et al. discussed the influence of initial water content of the PEM in power generation time [24]. In addition, Tajiri et al. and Chacko et al. reported that the cell IR behavior indicated that the water dehydrated from the PEM to the CL from the final point of the 2nd region to the final point of the 3rd region [24,26]. About a role as the water absorber of the ionomer, even if all of the ionomer at the anode and cathode were converted into membrane thickness, I/C = 1.0 and 1.5 would correspond to only 8 μm and 10 μm-thick membranes, respectively. Therefore, the existence of ionomer, as a water absorber,

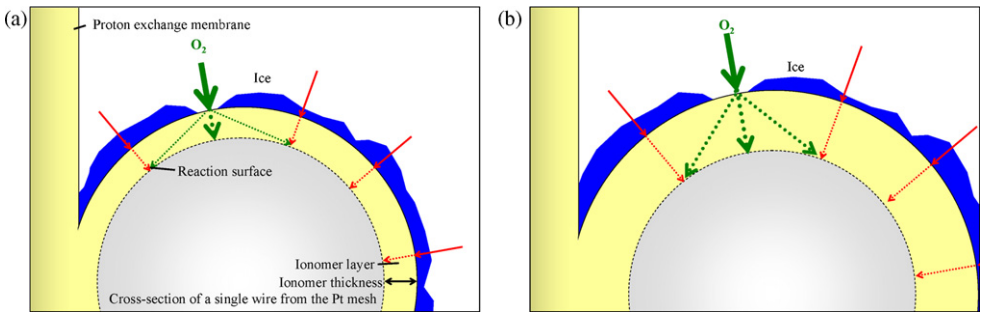

Fig. 11. Schematic image of oxygen transport under ice accumulation on the Pt mesh electrode. (a) and (b) show the oxygen transport through thin and thick ionomer layers over ice, respectively.

does not contribute significantly to prolonging the power generation time. Rather, the contribution of I/C to the prolongation of the power generation time does not originate from ionomer water uptake, but from ionomer oxygen transport. This is strongly supported by the results of the ex situ cold test conducted on the cell with a Pt mesh cathode. Fig. 11 shows a conceptual cross-section of the Pt mesh during the ex situ cold test, based on the results shown in Figs. 7 and 10. Oxygen dissolved into the ionomer around the Pt wire from the area not covered by ice, and diffused to the Pt surfaces, whether they were covered by ice or not. As can be inferred from the figure, if the ionomer layer is thin, oxygen diffuses difficultly through the ionomer from a region of the surface not covered by ice to a region of the Pt surface whose overlying ionomer is covered by ice, due to a decrease in the effective transport cross-section of the ionomer layer. As shown in Fig. 10(c), in the cell with a high I/C it is thought that oxygen dissolves into the ionomer facing the GDL, that it diffuses through the ionomer in the CL, and that it is used at the Pt reaction site. In addition, it is thought that the water produced at the Pt reaction sites diffuses to the pores in the GDL, that many microscopic ice particles are formed in the pores along the interface between the CL and the GDL, and that larger ice particles absorb smaller ones by repeated sublimation. Regarding the behavior of ice in the GDL, Sato et al. observed the sublimation of microscopic ice from the viewpoint of cold start-up of PEMFCs for automotive use [33]. They reported that the ice particles of relatively large size absorb those of relatively small size by repeated sublimation in the electrode. Thus, ionomer can function as a carrier of oxygen and water, and consequently a cell with a high I/C can continue to generate power for a long time.

In the 3rd region of Fig. 5, the cell voltage gradually decreased after the IR reached its minimum and began to increase, and its rate of decrease in the cell with an I/C = 1.5 was lower than that of the cell with I/C = 1.0. In this region, ice formed mainly in the GDL, because the amount of water produced in the CL was overwhelmingly larger than the pore volume, so that a large amount of the water produced was exhausted from the CL into the GDL through the ionomer. In this region of I/C = 1.5, the IR reached a constant value. This region, which was defined as the 4th region, appeared only for the cell with I/C = 1.5. The constant IR implies that the quantity of water was balanced between product water, water movement to the PEM, and water movement to the GDL.

4.3. Water in ionomer at −30 °C

Based on the discussion in Sections 4.1 and 4.2, it is reasonable to conclude that water in the PEM and ionomer does not freeze at −30 °C. This is consistent with the report by Saito et al. that water in PEM or ionomer does not freeze at −30 °C because it exists as bound water and it is influenced by nano-scale pores formed by sulfonic acid groups [34].

5. Conclusions

With the goal of improving the reliability of PEMFCs for automotive use, the influence of the ionomer content in the CL during cold start-up was studied at −30 °C in single cells. It was found that cold start-up performance and durability improved significantly at higher ionomer content in CL because of better oxygen permeation with ice formation in the CL. To obtain additional evidence of oxygen permeation through the ionomer, ex situ generation tests were conducted on sub-cells with cathodes consisting of ionomer-coated Pt mesh under the same ambient conditions. The sub-cell with thicker ionomer showed a smaller $\eta_{diffusion}$ with ice formation. The results indicate the importance of ionomer as a carrier of oxygen, protons, and water.

Acknowledgments

The authors express their thanks to all those who assisted in the writing of this report. This research was performed under a grant from the Water Management Project from the New Energy and Industrial Technology Development Organization (NEDO) for strategic technical development for the practical realization of PEMFCs.

References

[1] T. Morita, K. Kojima, ECS Trans. 16 (2) (2008) 185–198.
[2] Q. Yan, H. Toghiani, Y.W. Lee, K. Liang, H. Causey, J. Power Sources 160 (2006) 1242–1250.
[3] Y. Hishinuma, T. Chikahisa, F. Kagami, T. Ogawa, JSME Int. J. B 47 (2) (2004) 235–241.
[4] H. Shirato, H. Hoshina, Y. Yamakoshi, K. Tomita, Y. Oka, M. Yoshida, M. Yoshida, H. Kamata, M. Sakairi, T. Suda, Rep. Hokkaido Ind. Res. Inst. 305 (2006) 149–157.
[5] F. Jiang, C.Y. Wang, J. Electrochem. Soc. 155 (2008) B743–B751.
[6] E. Pinton, Y. Fourneron, S. Rosini, L. Antoni, J. Power Sources 186 (2009) 80–88.
[7] M. Khandelwal, S. Lee, M.M. Mench, J. Power Sources 172 (2007) 816–830.
[8] C. Rice-York, J. Needham, N. Gupta, P.L. Hagans, ECS Trans. 1 (6) (2006) 383–388.
[9] F. Jiang, W. Fang, C.Y. Wang, Electrochim. Acta 53 (2007) 610–621.
[10] S. Ge, C.Y. Wang, Electrochem. Solid-State Lett. 9 (11) (2006) A499–A503.
[11] Y. Ishikawa, T. Morita, M. Shiozawa, ECS Trans. 31 (2006) 889–895.
[12] Y. Ishikawa, T. Morita, K. Nakata, K. Yoshida, M. Shiozawa, J. Power Sources 163 (2007) 708–712.
[13] Y. Ishikawa, H. Hamada, M. Uehara, M. Shiozawa, J. Power Sources 179 (2008) 547–552.
[14] Y. Ishikawa, M. Shiozawa, M. Uehara, H. Hamada, Denso Tech. Rev. 13 (1) (2008) 31–36.
[15] J. Li, S. Lee, J. Roberts, Electrochim. Acta 53 (2008) 5391–5396.
[16] S. Ge, C.Y. Wang, J. Electrochem. Soc. 154 (12) (2007) B1399–B1406.
[17] H. Meng, Electrochim. Acta 53 (2008) 6521–6529.
[18] H. Meng, J. Power Sources 178 (2008) 141–150.
[19] H. Meng, Int. J. Hydrogen Energy 33 (2008) 5738–5747.
[20] L. Mao, J. Electrochem. Soc. 154 (2) (2007) B139–B146.
[21] Y. Wang, J. Electrochem. Soc. 154 (10) (2007) B1041–B1048.
[22] M. Oszcipok, D. Riemann, U. Kronenwett, M. Kreideweis, M. Zedda, J. Power Sources 145 (2005) 407–415.
[23] J. Hou, W. Song, H. Yu, Y. Fua, Z. Shao, B. Yi, J. Power Sources 171 (2007) 610–616.
[24] K. Tajiri, Y. Tabuchi, C.Y. Wang, J. Electrochem. Soc. 154 (2) (2007) B147–B152.
[25] K. Tajiri, Y. Tabuchi, F. Kagami, S. Takahashi, K. Yoshizawa, C.Y. Wang, J. Power Sources 165 (2007) 279–286.

[26] C. Chacko, R. Ramasamy, S. Kim, M. Khandelwal, M. Mencha, J. Electrochem. Soc. 155 (11) (2008) B1145–B1154.
[27] K. Tajiri, C.-Y. Wang, Y. Tabuchi, Electrochim. Acta 53 (2008) 6337–6343.
[28] S.-Y. Lee, S.-U. Kim, H.-J. Kim, J.H. Jang, I.-H. Oh, E.A. Cho, S.-A. Hong, J. Ko, T.W. Lim, K.Y. Lee, T.H. Lim, J. Power Sources 180 (2008) 784–790.
[29] K. Kawahara, S. Nagano, R&D Rev. Toyota CRDL 29 (4) (1994) 13–22.
[30] F.N. Büchi, M. Wakizoe, S. Srinivasan, J. Electrochem. Soc. 143 (3) (1996) 927–932.
[31] S. Mitsushima, N. Araki, N. Kamiya, K. Ota, J. Electrochem. Soc. 149 (10) (2002) A1370–A1375.
[32] H.F.M. Mohamed, K. Ito, Y. Kobayashi, N. Takimoto, Y. Takeoka, A. Ohira, Polymer 49 (2008) 3091–3097.
[33] T. Sato, I. Hasegawa, M. Hori, Proc. of the 49th Battery Symposium in Japan, 2008, p. 410.
[34] M. Saito, K. Hayamizu, T. Okada, J. Phys. Chem. B 109 (2005) 3112–3119.